

^{16}O scattering from the even- A Mg and Si isotopesH. T. Fortune,* A. Richter,[†] R. H. Siemssen,[‡] and J. L. Yntema*Argonne National Laboratory, Argonne, Illinois 60439*

(Received 24 April 1979)

Excitation functions for ^{16}O elastic scattering were measured for $^{24,26}\text{Mg}$ and $^{28,30}\text{Si}$ at several angles in the energy range $20 \text{ MeV} \lesssim E_{\text{c.m.}} \lesssim 35 \text{ MeV}$. Detailed angular distributions were obtained for ^{24}Mg (^{26}Mg) at $E_{\text{c.m.}} = 21$ (21.7), 24 (24.8), 27 (27.9), and 30 (31.0) MeV. The data were analyzed with a conventional optical model with a shallow, and energy-dependent real, and a weakly absorbing and energy-dependent imaginary potential.

NUCLEAR REACTIONS $^{24}\text{Mg}(^{16}\text{O}, ^{16}\text{O})$, $^{26}\text{Mg}(^{16}\text{O}, ^{16}\text{O})$, $^{28}\text{Si}(^{16}\text{O}, ^{16}\text{O})$, $^{30}\text{Si}(^{16}\text{O}, ^{16}\text{O})$. Measured elastic scattering cross section $20 \text{ MeV} \lesssim E_{\text{c.m.}} \lesssim 35 \text{ MeV}$. Fitted optical models to data.

I. INTRODUCTION

The elastic scattering of ^{16}O on a variety of light nuclei has long presented an interesting and informative field of study. All but the most recent work is summarized in Refs. 1 and 2. Two principal conclusions have emerged from these studies. First, when the conventional optical model is used to describe the data, all studies involving large amounts of angular-distribution and excitation-function data seem to require shallow real-well depths—in the range $V \sim 15\text{--}30 \text{ MeV}$ (attractive). Second, most of the effects seen in the scattering process seemed to be manifestations of the behavior of those angular momenta that correspond to grazing collisions. The absorptive potential must be made transparent for those l values; the details of the form and magnitude of W are highly ambiguous.

For elastic scattering of ^{16}O on nuclei near the middle of the sd shell, data have been reported for $^{16}\text{O} + ^{24}\text{Mg}$ (Refs. 3–5) and for $^{16}\text{O} + ^{28}\text{Si}$ (Refs. 6–10). Reference 3 contains an angular distribution at a bombarding energy of 60 MeV and excitation functions at two angles for the range $E = 47\text{--}72 \text{ MeV}$. Reference 4 measured excitation functions at three angles for $E = 25\text{--}64 \text{ MeV}$.

For $^{16}\text{O} + ^{28}\text{Si}$, Ref. 6 measured back-angle angular distributions at bombarding energies of 50 and 55 MeV, and Ref. 7 reported an excitation function at extreme backward angles for $E = 27\text{--}58 \text{ MeV}$. Shkolnik *et al.*⁹ measured detailed angular distributions at five bombarding energies between 45 and 63 MeV. Cramer *et al.*⁸ obtained and analyzed forward-angular-distribution data between 33 and 215 MeV. Strong oscillatory structure has been observed at extreme backward angles for $^{16}\text{O} + ^{28}\text{Si}$ (Refs. 6, 7) and $^{12}\text{C} + ^{28}\text{Si}$ (Ref. 10), and has been

given a variety of interpretations.^{6,7,11,12}

Because of this continuing interest, we present here an extensive body of angular-distribution and excitation-function data for the elastic scattering of ^{16}O on the even- A isotopes of Mg and Si. The data have never been published, but results^{13,17} of preliminary optical-model analysis of them have provided a basis for much of the subsequent work.

II. EXPERIMENTAL PROCEDURE

The experiments were performed at the Argonne National Laboratory. Targets were carbon-backed foils of Mg and SiO_2 , with isotopic enrichments of 99.96% (^{24}Mg), 98.78% (^{26}Mg), 99.38% (^{28}Si), and 95.55% (^{30}Si). Target thicknesses were typically $50\text{--}150 \mu\text{g}/\text{cm}^2$. A flash of gold on the targets aided in monitoring changes in their quality under bombardment, using monitor detectors placed at 10° on each side of the beam. No target deterioration was observed for beam currents $\leq 200 \text{ nA}$.

Kinematic coincidences were measured between the scattered ^{16}O ions and the recoiling target nuclei with five pairs of large-area ($10 \times 50 \text{ mm}$) detectors in a computer-controlled scattering chamber with four movable arms. The setup has been described previously.¹⁴ Solid angles of the detectors varied from $2 \times 10^{-4} \text{ sr}$ at forward angles to $2 \times 10^{-3} \text{ sr}$ at backward angles. The angle defining apertures (on the ^{16}O detectors) were kinematically curved and subtended a width of less than $\pm 0.5^\circ$ (lab) in the scattering plane. The apertures on the recoil detectors were made at least twice as wide as the angle defining apertures to assure 100% detection efficiency in the presence also of angular straggling.

Absolute cross sections were obtained by normalizing the forward-angle data at 35 MeV to

Rutherford scattering. Relative normalizations among the various detectors were obtained from comparison of yields at overlapping data points. Uncertainties in the relative cross sections as large as 30% could be present in the data. An additional difficulty was encountered for the ^{24}Mg target. Because of a large inelastic cross section, the spectra were sometimes contaminated with an inelastic peak. (For ^{24}Mg , kinematic effects are not sufficient to completely eliminate the inelastically scattered ^{16}O ions via coincidence). Peak-fitting procedures were used for the ^{24}Mg data to extract the relative elastic and inelastic contributions, but the presence of the inelastic peak may well have produced additional uncertainties in the $^{24}\text{Mg} + ^{16}\text{O}$ data at large angles and high energies.

To account for the change of the average charge of the incident ions as they passed through the target, the integrated beam current was corrected with the expression of Booth and Grant.¹⁵

For ^{24}Mg and ^{26}Mg , excitation functions were measured at six angles ($\theta_{\text{c.m.}} = 50^\circ, 60^\circ, 70^\circ, 80^\circ, 90^\circ,$ and 100°) in 250 or 500 keV steps (lab) over the bombarding energy range 30–54 MeV. In addition, angular distributions were measured for ^{24}Mg (^{26}Mg) at bombarding energies $E_{\text{c.m.}} = 21$ (21.7), 24 (24.8), 27 (27.9), and 30 (31) MeV over the c.m. angular range 20° – 110° .

For ^{28}Si and ^{30}Si , excitation functions were measured in 0.5 or 1.0 MeV steps (lab) over the bombarding energy range $22 \text{ MeV} \leq E_{\text{c.m.}} \leq 36 \text{ MeV}$ at five angles ($\theta_{\text{c.m.}} = 60^\circ, 70^\circ, 80^\circ, 90^\circ,$ and 100°).

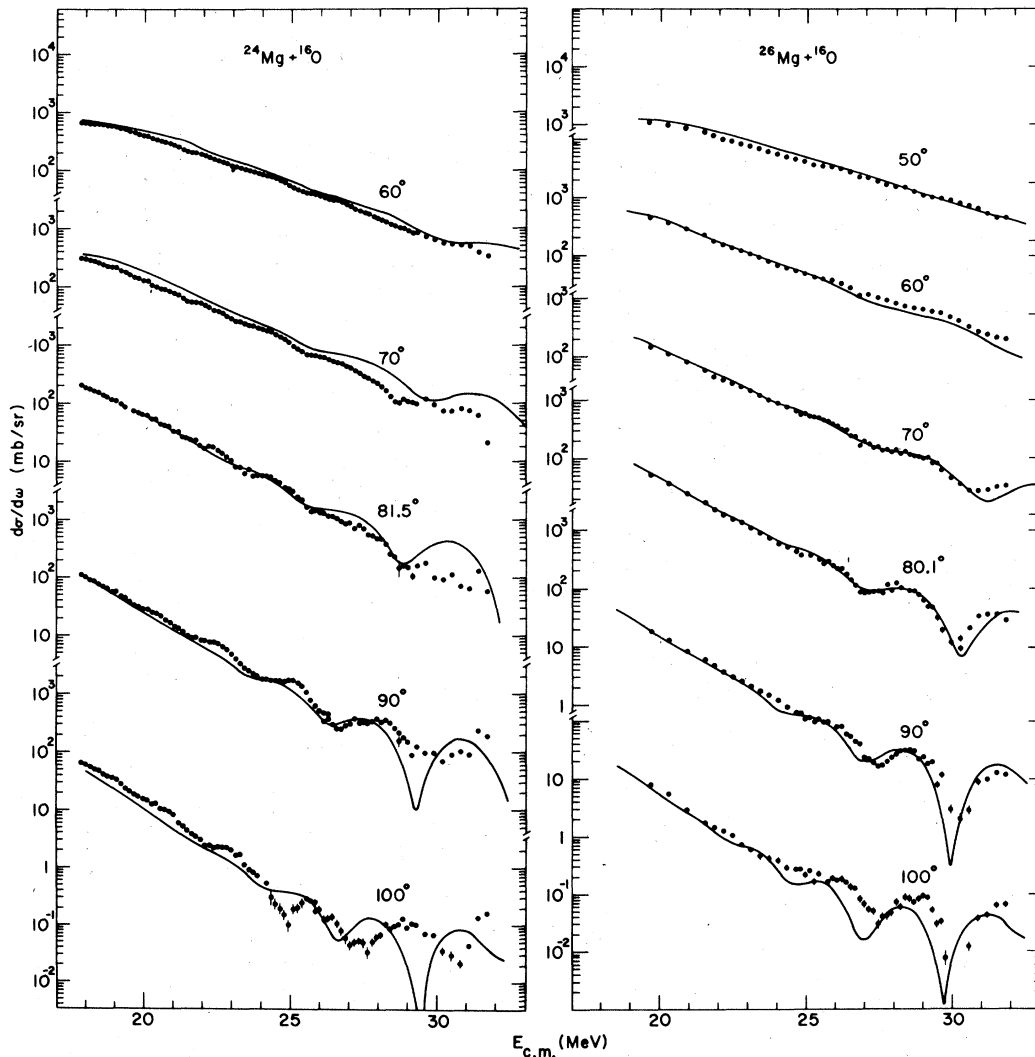


FIG. 1. Excitation functions for the elastic scattering of ^{16}O from ^{24}Mg (left) and ^{26}Mg (right). Curves are results of optical-model calculations with pot. M of Table I.

III. RESULTS AND ANALYSIS

The $^{24,26}\text{Mg} + ^{16}\text{O}$ excitation functions are displayed in Fig. 1, and the angular distributions in Fig. 2. The overall features of the data are very similar to those encountered in other studies of ^{16}O scattering. Angular distributions at the lower energies are smooth but the cross sections drop below Rutherford cross section at larger angles. As the energy is increased, this deviation from Rutherford scattering occurs at more forward angles, the overall slope of the angular distribu-

tions increases, and oscillations begin to appear. These effects are also apparent in the excitation functions. The larger the angle, the lower the energy at which oscillations appear. These oscillations are typical of diffraction structure and change smoothly as a function of angle or energy. Peak-to-valley ratios in excess of 10 are not uncommon. Close inspection of Figs. 1 and 2 reveals significant differences between the data from ^{24}Mg and from ^{26}Mg . Careful measurements of these data show that these differences are real. This point will be discussed further below in connection

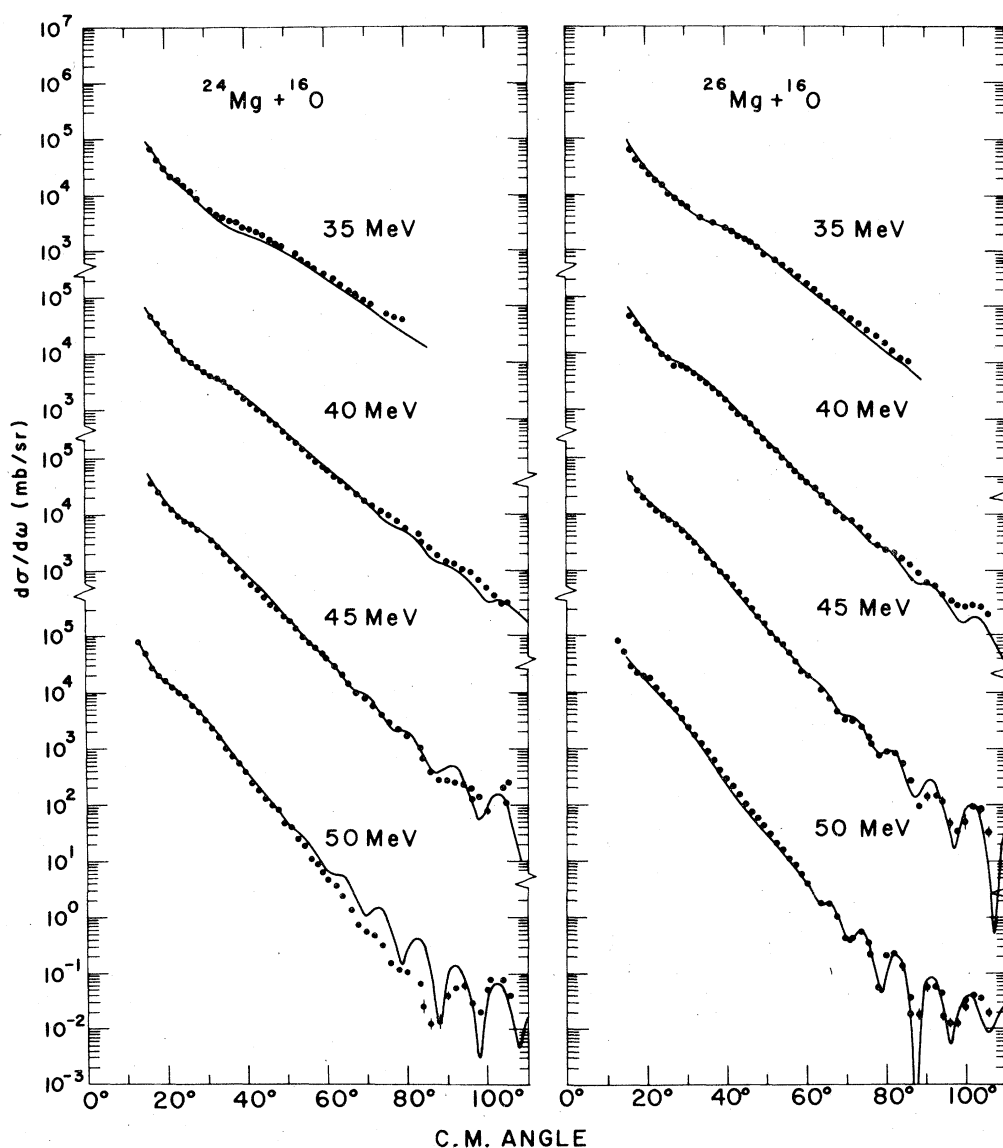


FIG. 2. Angular distributions for $^{16}\text{O} + ^{24}\text{Mg}$ (left) and $^{16}\text{O} + ^{26}\text{Mg}$ (right) compared with optical-model predictions of pot. M .

with the optical-model analysis.

Excitation functions for $^{28,30}\text{Si} + ^{16}\text{O}$ are displayed in Figs. 3 and 4. The structure observed here is similar to that for Mg, except that for Si, the oscillations begin at a higher energy—a consequence of the increased Coulomb barrier. The differences between the data for ^{28}Si and ^{30}Si are not as great as those for ^{24}Mg and ^{26}Mg . In fact, the Si data very closely resemble the $^{26}\text{Mg} + ^{16}\text{O}$ scattering, after the increased Coulomb barrier has been taken into account. By comparison of Figs. 3 and 1, one can see that the scattering from ^{28}Si and ^{26}Mg are more similar than the scattering from ^{24}Mg and ^{26}Mg . Thus it would appear that the four nuclei studied here the ^{24}Mg data are anomalous, whereas the other three sets of data are very similar. This point is discussed further below.

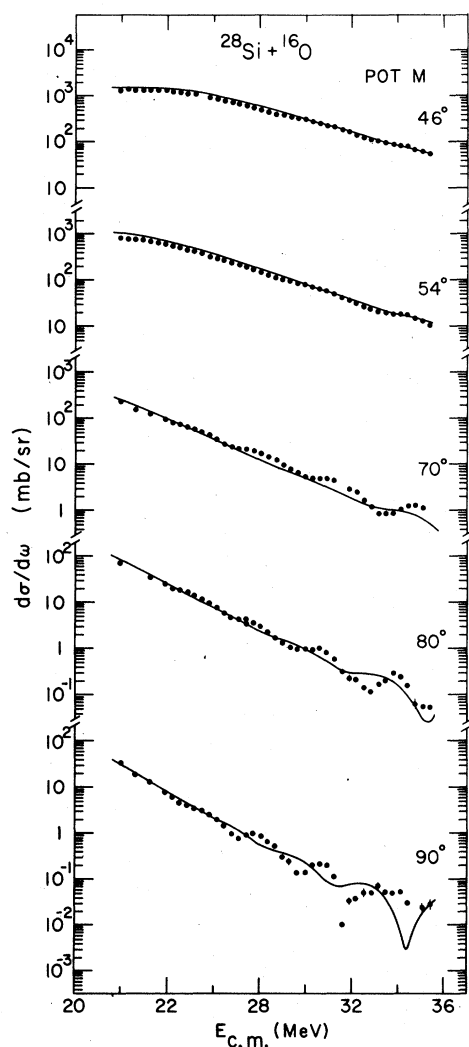


FIG. 3. Excitation functions for $^{16}\text{O} + ^{28}\text{Si}$ compared with predictions of pot. M .

The data were analyzed in terms of the conventional optical model, using the extensively modified version of the optical-model code ABACUS¹⁶ at Argonne. Both the real and imaginary potentials were taken to be Woods-Saxon shape.

Most of the early calculations centered on attempts to fit the Mg data. For a given angular distribution, it was always possible to find a number of different potentials that gave a reasonable account of the data. These included a range of real well depths ($V \sim 10\text{--}200$ MeV) and a range of imaginary well depths ($W \sim 2\text{--}60$ MeV). However, inspection of the best-fit potentials for the different angular distributions showed that most of the potentials did not possess a regular energy dependence—the parameters obtained at one energy

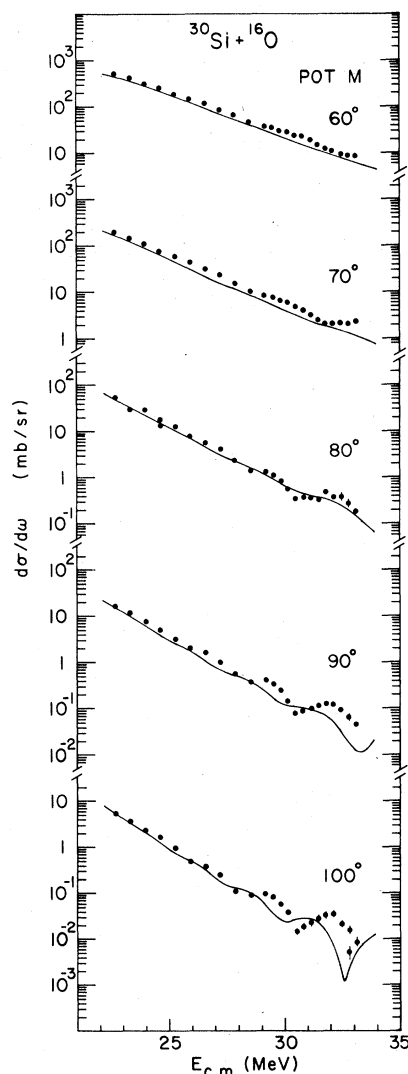


FIG. 4. Excitation functions for $^{16}\text{O} + ^{30}\text{Si}$ compared with predictions of pot. M .

TABLE I. Optical-model parameters for elastic scattering of ^{16}O from $^{24,26}\text{Mg}$ and $^{28,30}\text{Si}$. Strengths in MeV, lengths in fm.

Label	V	W	r_0^d	a_v	a_w
M^a	$7.5 + 0.5E_{\text{c.m.}}$	$0.4 + 0.15E_{\text{c.m.}}$	1.35	0.47	0.30
B^b	$12.0 + 0.25E_{\text{c.m.}}$	$0.4 + 0.15E_{\text{c.m.}}$	1.35	0.49	0.49
S^c	$7.5 + 0.5E_{\text{c.m.}}$	$-2.0 + 0.2E_{\text{c.m.}}$	1.35	0.49	0.32

^a Best-fit potential for $^{16}\text{O} + ^{26}\text{Mg}$.

^b From Ref. 14.

^c Best-fit potential for $^{16}\text{O} + \text{Si}$.

^d $R = r_0(A_1^{1/3} + A_2^{1/3})$.

bore little resemblance to those obtained at another energy. In addition, the potentials obtained for ^{24}Mg and ^{26}Mg were different. In fact, the ^{24}Mg data were always more difficult to fit than were

the ^{26}Mg data.

Thus the requirement of a consistent set of parameters at the different energies greatly reduced the available potentials. Attention was then

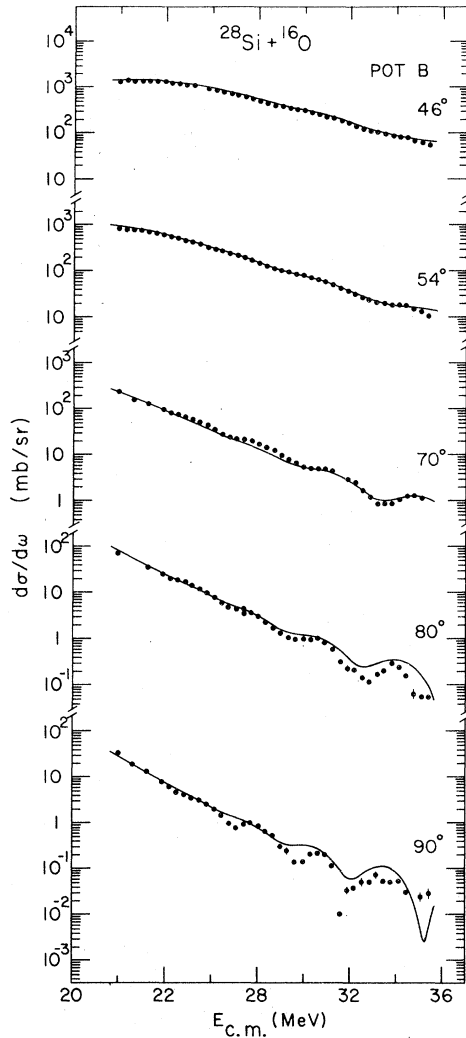


FIG. 5. Data of Fig. 3, compared with optical-model calculations using pot. B from Ref. 17.

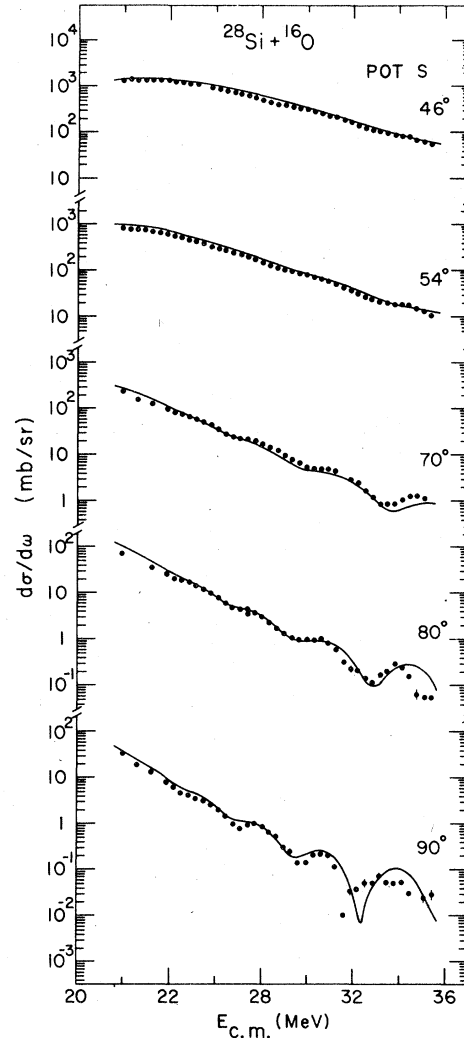


FIG. 6. Data of Fig. 3 compared with calculations with best-fit potential, S , of Table I.

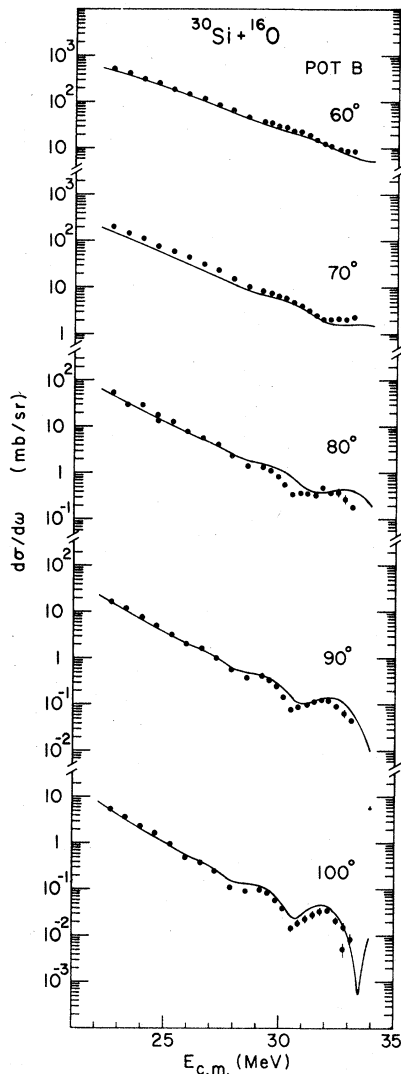


FIG. 7. Data for $^{16}\text{O} + ^{30}\text{Si}$ and calculations with pot. B.

focused on the excitation functions. Sets of optimum parameters were obtained via parameter scans rather than by searches. The quality of the fits was determined by eye rather than by a requirement of a minimum χ^2 . The technique usually works better in the absence of "perfect" fits. It was not possible to find a potential with a smooth energy dependence that gave a good fit to the $^{24}\text{Mg} + ^{16}\text{O}$ excitation functions. The potential (pot. M) which gave the best fit to the $^{26}\text{Mg} + ^{16}\text{O}$ excitation functions is given in Table I. Cross sections calculated with this potential are compared with the excitation function data in Fig. 1 for both ^{24}Mg and ^{26}Mg . This potential also gives reasonable agreement with the $^{26}\text{Mg} + ^{16}\text{O}$ angular distributions, as can be seen from Fig. 2. It was observed that parameters which give good fits to the excitation

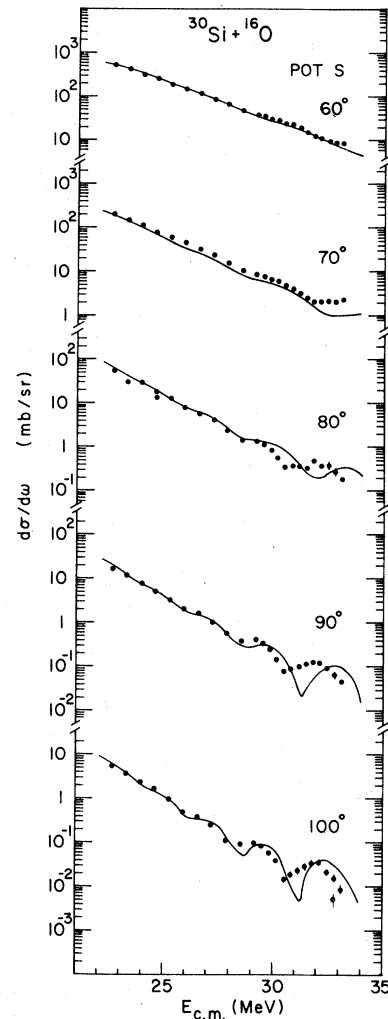


FIG. 8. Data for $^{16}\text{O} + ^{30}\text{Si}$ and calculations with pot. S.

functions usually also fit the angular distributions, whereas the converse is not true.

This final potential is quite similar to the one obtained from fits to ^{16}O scattering from lighter targets—in particular $^{14,15}\text{N}$ (Refs. 17, 18). It is characterized by a shallow real potential that increases in depth with bombarding energy and by weak absorption. Strongly-absorbing potentials were less satisfactory.

The final $^{16}\text{O} + ^{26}\text{Mg}$ potential, however, does not give a good account of the $^{16}\text{O} + ^{24}\text{Mg}$ data, as is apparent from Figs. 1 and 2. No potential was discovered that could account for the $^{24}\text{Mg} + ^{16}\text{O}$ data over the full angular and energy range covered in the present work. This consistent failure to fit the ^{24}Mg data, together with the distinct differences between the ^{24}Mg data and the other data reported herein, may indicate that the $^{24}\text{Mg} + ^{16}\text{O}$ elastic scattering contains contributions from

processes other than simple potential scattering. For example, the observation of large inelastic cross sections to the 1.37-MeV 2^+ state would indicate that two-step processes may be important (Ref. 5). In fact, our pot. M has been reasonably successful in coupled-channel calculations⁴ for limited data on $^{24}\text{Mg} + ^{16}\text{O}$ elastic and inelastic excitation functions.

Despite the similarities between the ^{26}Mg and ^{28}Si data, the potential that gave a good account of the $^{26}\text{Mg} + ^{16}\text{O}$ scattering gave less satisfactory results for $^{28}\text{Si} + ^{16}\text{O}$, as can be seen in Fig. 3. Calculations with parameters obtained from fitting very extensive $^{18}\text{O} + ^{16}\text{O}$ scattering data,¹⁴ however, produced reasonable agreement for $^{28}\text{Si} + ^{16}\text{O}$. These results are displayed in Fig. 5. Pot. B is the $^{18}\text{O} + ^{16}\text{O}$ potential,¹⁴ which is also listed in Table I.

Attempts to obtain a best-fit potential for $^{28}\text{Si} + ^{16}\text{O}$ led to parameters somewhat different from those above, viz. pot. S of Table I. Calculations with this parameter set are shown in Fig. 6. This is a weakly-absorbing potential. Calculations with a strongly-absorbing potential gave poor agreement. These $^{16}\text{O} + ^{28}\text{Si}$ parameters were used to generate theoretical curves for $^{30}\text{Si} + ^{16}\text{O}$ scatter-

ing. The agreement (Figs. 4, 7, 8) is not impressive, but is satisfactory.

IV. DISCUSSION AND CONCLUSIONS

The data reported here exhibit oscillations very similar to, but less pronounced than, the structure observed^{6,7} at more backward angles in $^{16}\text{O} + ^{28}\text{Si}$. It is very likely that they possess a common origin. Dehnhard, Shkolnik, and Franey¹² have demonstrated that the 180° excitation structure can be well fitted with an optical-model calculation utilizing a surface transparent potential with a reasonable energy dependence, but with the addition of a small parity-dependent term.

Except for the parity-dependent term, their potential is very similar to those found here. In fact, potentials of this type fit amazingly well the detailed $^{16}\text{O} + ^{28}\text{Si}$ angular distributions of Ref. 9. On the other hand, the global energy-independent potential of Ref. 8 which works quite well at high energies (above about 100 MeV) and at forward angles fails completely to reproduce the oscillations in the lower-energy data, even at reasonably forward angles.

*Present address: University of Pennsylvania, Philadelphia, Pa. 19104

†Present address: Institut für Kernphysik, Technische Hochschule Darmstadt, 6100 Darmstadt, W. Germany.

‡Present address: K.V.I., Groningen, The Netherlands.

¹R. H. Siemssen, in *Nuclear Molecular Phenomena*, edited by N. Cindro (North-Holland, Amsterdam, 1978), p. 61.

²A. Richter and C. Toepffer, in *Heavy Ion Collisions*, edited by R. Bock (North-Holland, Amsterdam, in press).

³K. Siwek-Wilczyńska, J. Wilczyński, and P. R. Christensen, Nucl. Phys. **A229**, 461 (1974).

⁴W. Mittig, P. Charles, S. M. Lee, I. Badawy, B. Berthier, B. Fernandes, and J. Gastebois, Nucl. Phys. **A233**, 48 (1974).

⁵J. Carter, R. G. Clarkson, V. Hnizdo, R. J. Keddy, D. W. Mingay, F. Osterfeld, and J. P. F. Sellschop, Nucl. Phys. **A273**, 523 (1976).

⁶P. Braun-Munzinger, G. M. Berkowitz, T. M. Cormier, C. M. Jachinski, J. W. Harris, J. Barrette, and M. J. Levine, Phys. Rev. Lett. **38**, 944 (1977).

⁷J. Barrette, M. J. Levine, P. Braun-Munzinger, G. M. Berkowitz, M. Gai, J. W. Harris, and C. M. Jachinski, Phys. Rev. Lett. **40**, 445 (1978).

⁸J. C. Cramer, R. M. DeVries, D. A. Goldberg, M. S. Zisman and C. F. Maguire, Phys. Rev. C **14**, 2158 (1976).

⁹V. Shkolnik, D. Dehnhard, S. Kubono, M. A. Franey, and S. Tripp, Phys. Lett. **74B**, 195 (1978).

¹⁰J. Carter, R. G. Clarkson, V. Hnizdo, and J. P. F. Sellschop, Nucl. Phys. **A297**, 520 (1978).

¹¹M. R. Clover, R. M. DeVries, R. Ost, N. J. A. Rust, R. N. Cherry, Jr., and H. E. Gove, Phys. Rev. Lett. **40**, 1008 (1978).

¹²D. Dehnhard, V. Shkolnik, and M. A. Franey, Phys. Rev. Lett. **40**, 1549 (1978).

¹³R. H. Siemssen, in Proceedings of the Symposium on Heavy Ion Scattering, Argonne National Laboratory, Report No. ANL-7837, 1971, p. 145.

¹⁴R. H. Siemssen, H. T. Fortune, A. Richter, and J. W. Tippie, Phys. Rev. C **5**, 1839 (1972).

¹⁵W. Booth and I. S. Grant, Nucl. Phys. **63**, 481 (1965), as corrected in Ref. 14.

¹⁶S. Zawadski (unpublished).

¹⁷R. H. Siemssen, H. T. Fortune, R. Malmin, A. Richter, J. W. Tippie, and P. P. Singh, Phys. Rev. Lett. **25**, 536 (1970).

¹⁸R. E. Malmin, Ph.D. thesis, Indiana University, 1972 (unpublished).